Received 5 April 2015
Revised 1 June 2015
Accepted 2 June 2015

Free convection in a square porous cavity filled with a nanofluid using thermal non equilibrium and Buongiorno models

Ioan Pop
Department of Mathematics, University of Cluj, Cluj, Romania
Mohammad Ghalambaz
Department of Mechanical Engineering, Dezful Branch, Islamic Azad University, Dezful, Iran, and
Mikhail Sheremet
Department of Theoretical Mechanics, Tomsk State University, Tomsk, Russian Federation

Abstract

Purpose – The purpose of this paper is to theoretically analysis the steady-state natural convection flow and heat transfer of nanofluids in a square enclosure filled with a porous medium saturated with a nanofluid considering local thermal non-equilibrium (LTNE) effects. Different local temperatures for the solid phase of the nanoparticles, the solid phase of porous matrix and the liquid phase of the base fluid are taken into account.

Design/methodology/approach – The Buongiorno's model, incorporating the Brownian motion and thermophoresis effects, is utilized to take into account the migration of nanoparticles. Using appropriate non-dimensional variables, the governing equations are transformed into the non-dimensional form, and the finite element method is utilized to solve the governing equations.

Findings – The results show that the increase of buoyancy ratio parameter (Nr) decreases the magnitude of average Nusselt number. The increase of the nanoparticles-fluid interface heat transfer parameter (Nhp) increases the average Nusselt number for nanoparticles and decreases the average Nusselt number for the base fluid. The nanofluid and porous matrix with large values of modified thermal capacity ratios (γ_f and γ_s) are of interest for heat transfer applications.

Originality/value – The three phases of nanoparticles, base fluid and the porous matrix are in the LTNE. The effect of mass transfer of nanoparticles due to the Brownian motion and thermophoresis effects are also taken into account.

Keywords Nanofluids, Free convection

Paper type Research paper

Nomenclature

Latin Symbols

C	nanoparticle volume fraction	C_0	ambient nanoparticle volume fraction
		D_B	Brownian diffusion coefficient

This work of M.A. Sheremet was conducted as a government task of the Ministry of Education and Science of the Russian Federation, Project Number 13.1919.2014/K.M. Ghalambaz is thankful to Dezful Branch, Islamic Azad University, Dezful, Iran and the Iran Nanotechnology Initiative Council (INIC) for their supports. The authors also wish to express their thanks to the very competent reviewers for the valuable comments and suggestions.

International Journal of Numerical Methods for Heat & Fluid Flow
Vol. 26 No. 3/4, 2016
pp. 671-693

0961-5539
DOI 10.1108/HFF-04-2015-0133

D_T	thermophoretic diffusion coefficient
$\mathbf{g}$	gravitational acceleration vector
h_{fp}	interface heat transfer coefficient between the fluid/particle phases
h_{fs}	interface heat transfer coefficient between the fluid/solid-matrix phases
K	permeability of the porous medium
k	effective thermal conductivity
L	cavity size
Le	Lewis number
Nb	Brownian motion parameter
Nhp	Nield number for the fluid/nanoparticle interface (fluid/nanoparticle interface parameter)
Nhs	Nield number for the fluid/solid-matrix interface (fluid/solid-matrix interface parameter)
Nr	buoyancy ratio parameter
Nt	thermophoresis parameter
Nu	local Nusselt number
$\overline{Nu}$	average Nusselt number
p	pressure
Ra	thermal Rayleigh–Darcy number $Ra = (1-C_0)gK\rho_{f0}\beta\Delta TL/(\alpha_f\mu)$
Sh	local Sherwood number
$\overline{Sh}$	average Sherwood number
T	dimensional temperature
T_c	temperature at the right wall
T_h	temperature at the left wall
$\mathbf{V}$	Darcy velocity
$\overline{x}, \overline{y}$	Cartesian coordinates
$\overline{u}, \overline{v}$	the velocity components along $\overline{x}, \overline{y}$ directions

Greek symbols

α	effective thermal diffusivity
β	thermal expansion coefficient
γ_p	modified particle heat capacity
γ_s	modified porous solid-matrix thermal conductivity
ε	porosity
ε_p	modified diffusivity ratio
θ	dimensionless temperature
μ	dynamic viscosity
ρ	fluid density
(ρc)	effective heat capacity
τ	parameter defined by $\tau = (\rho c)_p/(\rho c)_f$
ϕ	relative nanoparticle volume fraction
ψ	dimensionless stream function
$\overline{\psi}$	dimensional stream function

Subscripts

0	the ambient property
f	base fluid phase
p	nanoparticle phase
s	porous medium solid-matrix phase

1. Introduction

The free convection in enclosures filled with a porous medium saturated with a fluid occurs in many industrial applications including electronic component cooling, geothermal systems and paper production. In free convection flow there is no need of any external work source or fan and the fluid moves due to the temperature difference in the enclosure. Designing a system relying on a natural convection heat transfer reduces the risk of the mechanical system failure because of the absence of any external power supply. It also reduces the induced noise because of the fans. Because of such advantages many of engineers and researchers are interested in analysis of the natural convection phenomena and the systems working based on the natural convection heat transfer.

In many natural convection applications when the thermal conductivity of the porous medium is comparatively low or the interaction between the fluid and the porous medium is high, it can be assumed that the temperature of the fluid and the solid porous matrix are very close or they are in local thermal equilibrium (LTE). This assumption simplifies the problem in such a way that the fluid and the porous matrix can be seen as a uniform mixture. However, there are many practical cases of natural convection in porous media with high thermal removal capacities, in which there are significant temperature differences between the porous matrix and the fluid inside

the pores. In these cases, the LTE assumption is no longer valid, and the local thermal non-equilibrium (LTNE) model for the porous medium and the fluid should be taken into account (Ingham and Pop, 2005; Baytaş and Pop, 2002).

Recently, new-engineered fluids containing nanoparticles, namely, nanofluids, are developed to enhance the thermal conductivity of the working fluid (see Abu-Nada and Chamkha, 2010; Basak and Chamkha, 2012; Nasrin *et al.*, 2012, 2014; Chamkha and Abu-Nada, 2012). Experiments indicate that the presence of nanoparticles in the base fluid results in augmentation of the thermal conductivity. The increase in the thermal conductivity of a fluid increases the thermal diffusivity, and hence, it could results in heat transfer enhancement in convective heat transfer systems. Therefore, the nanofluids are potential candidates for convective heat transfer enhancement in applications with high demand of the thermal energy removal. There are also applications in which the presence of nanoparticles induces other desired effects beyond the heat transfer enhancement. For example, the presence of zinc oxide or titanium dioxide nanoparticles in water shows inherent antibacterial effects (Zhang *et al.*, 2008; Hirota *et al.*, 2010). The presence of ceramic oxide (Choi *et al.*, 2008) or diamond nanoparticles (Saidur *et al.*, 2011) enhance the dielectric properties of the base fluid, which is of interest in electrical power transformers.

The experiments indicate that the presence of nanoparticles in a fluid affects the other thermo-physical properties such as dynamic viscosity and heat capacity of the resulting fluid (Khanafer and Vafai, 2011). This is while the convective heat transfer of nanofluids is affected by the thermal conductivity, the dynamic viscosity and other thermo-physical properties as well as the fluid flow characteristics or mass transfer mechanisms. Therefore, the analysis of convective heat transfer of nanofluids, considering changes in thermo-physical properties and heat transfer mechanisms is highly demanded for engineering applications of nanofluids. Buongiorno (2006) analyzed the nanoparticles mass transfer in nanofluids using scale analysis and found that the Brownian motion and thermophoresis are two dominant particle transfer mechanisms in nanofluids. The Brownian motion force tends to uniform nanoparticles in the fluid. The thermophoresis force originates from the temperature gradient in the base fluid. When the size of a particle is very fine (in the order of nanometer), the particle receives more momentum impacts from the fluid molecules in hot side than that of the cold side; hence, the particle tends to move in a direction opposite to the temperature gradient (the particle moves from hot to cold). Therefore, there are mass transfer mechanisms in nanofluids because of the Brownian motion and thermophoresis forces. The migrated nanoparticles carry energy and transfer it to the surrounding medium. When the thermal conductivity of the base fluid is very low, the quiescent fluid around the nanoparticle cannot adequately absorb the heat from the nanoparticle, and hence, the nanoparticles and the base fluid could be in local thermal non-equilibrium.

The natural convection heat transfer of a regular fluid in an enclosure using LTE model has been well studied by previous fundamental researches. For example, Baytaş and Pop (1999, 2001) studied the natural convection of a regular fluid in enclosures using LTE model. Choi *et al.* (1998) have considered the non-Darcy effects in natural convection of regular fluids in enclosures filled with a porous medium. Varol *et al.* (2008) conducted a numerical study to analysis the effect of the shape of the enclosure on the natural convective heat transfer of nanofluids.

The LTNE natural convection of a regular fluid in an enclosure has been investigated by Baytaş and Pop (2002). The heat transfer of nanofluid in porous media

using LTE was formulated by Nield and Kuznetsov (2009a, b) considering the Buongiorno's (2006) mathematical model. They (Nield and Kuznetsov, 2009a) analyzed the heat and mass transfer of nanofluids over a flat plate embedded in a Darcy porous medium using a similarity solution approach. Nield and Kuznetsov (2009b) have utilized the Buongiorno's mathematical model to analysis the linear stability of nanofluids between two infinite plates using LTE model. Later, Bhadauria and Agarwal (2011) have developed the model of Nield and Kuznetsov (2009b) to study the natural convection instability of nanofluids between two infinity plates using the LTNE model. Very recently, Sheremet and Pop (2014, 2015) utilized the Buongiorno's model developed by Nield and Kuznetsov (2009a, b) to analysis the natural convection heat transfer of nanofluids in an enclosure.

The present study aims to analysis the natural convection flow and heat transfer of nanofluids using the LTNE model considering the Buongiorno's model. In the present study, the three phases of nanoparticles, base fluid and the porous matrix are in the LTNE. The effect of mass transfer of nanoparticles due to the Brownian motion and thermophoresis effects are also taken into account.

2. Basic equations

Consider the steady free convection in a two-dimensional porous square cavity filled with a water-based nanofluid. It is assumed that nanoparticles are suspended in the nanofluid using either surfactant or surface charge technology. This prevents nanoparticles from agglomeration and deposition on the porous matrix (Kuznetsov and Nield, 2010, 2013; Nield and Kuznetsov, 2009a, 2014). A schematic view of the geometry of the problem under investigation is shown in Figure 1, where $\overline{x}$ and $\overline{y}$ are the Cartesian coordinates and L is the size of the cavity.

It is assumed that the left vertical wall is heated and maintained at the constant temperature T_h, while the right vertical wall is cooled and has the constant temperature T_c. The horizontal walls are adiabatic $\left(\partial T/\partial \overline{y}\right) = 0$, where T is the temperature. The Darcy-Boussinesq approximation and the LTNE between the fluid and solid-matrix and fluid and particle phase have been considered, thus heat flow has been described using three temperature model.

The conservation equations for the total mass, momentum, thermal energy in the fluid phase, thermal energy in the particle phase, thermal energy in the solid-matrix phase, and nanoparticles, come out to be as below. A detailed derivation of these

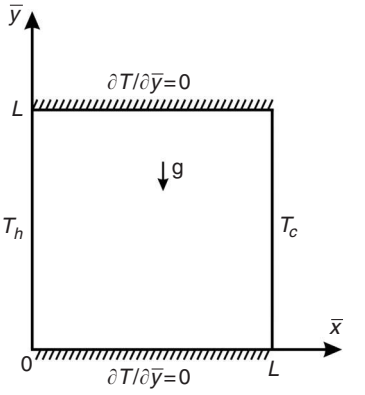

Figure 1.
Physical model and coordinate system

equations has been dealt by Buongiorno (2006), Tzou (2008a, b), Nield and Kuznetsov (2009a), and Kuznetsov and Nield (2010):

$$\nabla \cdot \mathbf{V} = 0 \tag{1}$$

$$\frac{\mu}{K}\mathbf{V} = -\nabla p + \left[C\rho_p + (1-C)\rho_{f0}\left(1-\beta\left(T_f - T_c\right)\right)\right]\mathbf{g} \tag{2}$$

$$\frac{1}{\varepsilon}\mathbf{V}\cdot\nabla T_f = \frac{k_f}{(\rho\, c)_f}\nabla^2 T_f + \tau\left(D_B \nabla C\cdot\nabla T_f + \frac{D_T}{T_c}\nabla T_f \cdot \nabla T_f\right) + \frac{\left[h_{fp}\left(T_p - T_f\right) + h_{fs}\left(T_s - T_f\right)\right]}{\varepsilon(1-C_0)(\rho c)_f} \tag{3}$$

$$\frac{1}{\varepsilon}\mathbf{V}\cdot\nabla T_p = \frac{k_p}{(\rho c)_p}\nabla^2 T_p + \frac{h_{fp}}{\varepsilon C_0 (\rho c)_p}\left(T_f - T_p\right) \tag{4}$$

$$0 = \frac{k_s}{(\rho c)_s}\nabla^2 T_s + \frac{h_{fs}}{(1-\varepsilon)(\rho c)_s}\left(T_f - T_s\right) \tag{5}$$

$$\frac{1}{\varepsilon}\mathbf{V}\cdot\nabla C = D_B \nabla^2 C + \frac{D_T}{T_c}\nabla^2 T_f \tag{6}$$

In these equations, both Brownian transport and thermophoresis coefficients are taken to be time-independent, in tune with the recent studies that neglect the effect of thermal transport attributed to the small size of the nanoparticles (as per recent arguments by Keblinski and Cahill, 2005). Further, thermophoresis and Brownian transport coefficients are assumed to be temperature-independent due to the fact that the temperature ranges under consideration are not far away from the critical value, and the volume averages over a representative elementary volume.

Equations (1)-(6) for the problem under consideration can be written in dimensional Cartesian coordinates $\overline{x}, \overline{y}$ taking into account the slow flow and dilute nanoparticle concentration as:

$$\frac{\partial \overline{u}}{\partial \overline{x}} + \frac{\partial \overline{v}}{\partial \overline{y}} = 0 \tag{7}$$

$$\frac{\partial p}{\partial \overline{x}} = -\frac{\mu}{K}\overline{u} \tag{8}$$

$$\frac{\partial p}{\partial \overline{y}} = -\frac{\mu}{K}\overline{v} - \left[C\left(\rho_p - \rho_{f0}\right) + \rho_{f0}\left(1-\beta\left(T_f - T_c\right)(1-C_0)\right)\right]g \tag{9}$$

$$\frac{1}{\varepsilon}\left(\overline{u}\frac{\partial T_f}{\partial \overline{x}} + \overline{v}\frac{\partial T_f}{\partial \overline{y}}\right) = \alpha_f\left(\frac{\partial^2 T_f}{\partial \overline{x}^2} + \frac{\partial^2 T_f}{\partial \overline{y}^2}\right) + \tau\left\{D_B\left(\frac{\partial C}{\partial \overline{x}}\frac{\partial T_f}{\partial \overline{x}} + \frac{\partial C}{\partial \overline{y}}\frac{\partial T_f}{\partial \overline{y}}\right) + \left(\frac{D_T}{T_c}\right)\left[\left(\frac{\partial T_f}{\partial \overline{x}}\right)^2 + \left(\frac{\partial T_f}{\partial \overline{y}}\right)^2\right]\right\}$$

$$+\frac{\left[h_{fp}(T_p-T_f)+h_{fs}(T_s-T_f)\right]}{\varepsilon(1-C_0)(\rho c)_f} \tag{10}$$

$$\frac{1}{\varepsilon}\left(\overline{u}\frac{\partial T_p}{\partial \overline{x}}+\overline{v}\frac{\partial T_p}{\partial \overline{y}}\right)=\alpha_p\left(\frac{\partial^2 T_p}{\partial \overline{x}^2}+\frac{\partial^2 T_p}{\partial \overline{y}^2}\right)+\frac{h_{fp}}{\varepsilon C_0(\rho c)_p}(T_f-T_p) \tag{11}$$

$$0=\alpha_s\left(\frac{\partial^2 T_s}{\partial \overline{x}^2}+\frac{\partial^2 T_s}{\partial \overline{y}^2}\right)+\frac{h_{fs}}{(1-\varepsilon)(\rho c)_s}(T_f-T_s) \tag{12}$$

$$\frac{1}{\varepsilon}\left(\overline{u}\frac{\partial C}{\partial \overline{x}}+\overline{v}\frac{\partial C}{\partial \overline{y}}\right)=D_B\left(\frac{\partial^2 C}{\partial \overline{x}^2}+\frac{\partial^2 C}{\partial \overline{y}^2}\right)+\left(\frac{D_T}{T_c}\right)\left(\frac{\partial^2 T_f}{\partial \overline{x}^2}+\frac{\partial^2 T_f}{\partial \overline{y}^2}\right) \tag{13}$$

where $\overline{u},\overline{v}$ are the velocity components along $\overline{x},\overline{y}$ directions, respectively.

Introducing a stream function $\overline{\psi}$ defined by:

$$\overline{u}=\frac{\partial \overline{\psi}}{\partial \overline{y}},\quad \overline{v}=-\frac{\partial \overline{\psi}}{\partial \overline{x}}, \tag{14}$$

so that Equation (7) is satisfied identically. We are then left with the following equations:

$$\frac{\partial^2 \overline{\psi}}{\partial \overline{x}^2}+\frac{\partial^2 \overline{\psi}}{\partial \overline{y}^2}=-\frac{(1-C_0)\rho_{f0}gK\beta}{\mu}\frac{\partial T_f}{\partial \overline{x}}+\frac{\rho_p-\rho_{f0}}{\mu}gK\frac{\partial C}{\partial \overline{x}}, \tag{15}$$

$$\begin{aligned}\frac{1}{\varepsilon}\left(\frac{\partial \overline{\psi}}{\partial \overline{y}}\frac{\partial T_f}{\partial \overline{x}}-\frac{\partial \overline{\psi}}{\partial \overline{x}}\frac{\partial T_f}{\partial \overline{y}}\right)&=\alpha_f\left(\frac{\partial^2 T_f}{\partial \overline{x}^2}+\frac{\partial^2 T_f}{\partial \overline{y}^2}\right)+\tau\left\{D_B\left(\frac{\partial C}{\partial \overline{x}}\frac{\partial T_f}{\partial \overline{x}}+\frac{\partial C}{\partial \overline{y}}\frac{\partial T_f}{\partial \overline{y}}\right)\right.\\&\left.+\left(\frac{D_T}{T_c}\right)\left[\left(\frac{\partial T_f}{\partial \overline{x}}\right)^2+\left(\frac{\partial T_f}{\partial \overline{y}}\right)^2\right]\right\}\\&+\frac{\left[h_{fp}(T_p-T_f)+h_{fs}(T_s-T_f)\right]}{\varepsilon(1-C_0)(\rho c)_f}\end{aligned} \tag{16}$$

$$\frac{1}{\varepsilon}\left(\frac{\partial \overline{\psi}}{\partial \overline{y}}\frac{\partial T_p}{\partial \overline{x}}-\frac{\partial \overline{\psi}}{\partial \overline{x}}\frac{\partial T_p}{\partial \overline{y}}\right)=\alpha_p\left(\frac{\partial^2 T_p}{\partial \overline{x}^2}+\frac{\partial^2 T_p}{\partial \overline{y}^2}\right)+\frac{h_{fp}}{\varepsilon C_0(\rho c)_p}(T_f-T_p) \tag{17}$$

$$0=\alpha_s\left(\frac{\partial^2 T_s}{\partial \overline{x}^2}+\frac{\partial^2 T_s}{\partial \overline{y}^2}\right)+\frac{h_{fs}}{(1-\varepsilon)(\rho c)_s}(T_f-T_s) \tag{18}$$

$$\frac{1}{\varepsilon}\left(\frac{\partial \overline{\psi}}{\partial \overline{y}}\frac{\partial C}{\partial \overline{x}}-\frac{\partial \overline{\psi}}{\partial \overline{x}}\frac{\partial C}{\partial \overline{y}}\right)=D_B\left(\frac{\partial^2 C}{\partial \overline{x}^2}+\frac{\partial^2 C}{\partial \overline{y}^2}\right)+\left(\frac{D_T}{T_c}\right)\left(\frac{\partial^2 T_f}{\partial \overline{x}^2}+\frac{\partial^2 T_f}{\partial \overline{y}^2}\right) \tag{19}$$

Introducing the following dimensionless variables:

$$\begin{aligned}&x=\overline{x}/L,\quad y=\overline{y}/L,\quad \psi=\overline{\psi}/\alpha_f,\quad \phi=C/C_0,\\&\theta_f=(T_f-T_c)/\Delta T,\quad \theta_p=(T_p-T_c)/\Delta T,\quad \theta_s=(T_s-T_c)/\Delta T\end{aligned} \tag{20}$$

where $\Delta T=T_h-T_c$, and substituting (20) into Equations (15)-(19), we obtain:

$$\frac{\partial^2\psi}{\partial x^2}+\frac{\partial^2\psi}{\partial y^2}=-Ra\frac{\partial\theta_f}{\partial x}+Ra\cdot Nr\frac{\partial\phi}{\partial x} \tag{21}$$

$$\frac{\partial\psi}{\partial y}\frac{\partial\theta_f}{\partial x}-\frac{\partial\psi}{\partial x}\frac{\partial\theta_f}{\partial y}=\varepsilon\left(\frac{\partial^2\theta_f}{\partial x^2}+\frac{\partial^2\theta_f}{\partial y^2}\right)+Nb\left(\frac{\partial\phi}{\partial x}\frac{\partial\theta_f}{\partial x}+\frac{\partial\phi}{\partial y}\frac{\partial\theta_f}{\partial y}\right)+Nt\left[\left(\frac{\partial\theta_f}{\partial x}\right)^2+\left(\frac{\partial\theta_f}{\partial y}\right)^2\right]+Nhp\left(\theta_p-\theta_f\right)+Nhs\left(\theta_s-\theta_f\right) \tag{22}$$

$$\frac{\partial\psi}{\partial y}\frac{\partial\theta_p}{\partial x}-\frac{\partial\psi}{\partial x}\frac{\partial\theta_p}{\partial y}=\varepsilon_p\left(\frac{\partial^2\theta_p}{\partial x^2}+\frac{\partial^2\theta_p}{\partial y^2}\right)+Nhp\cdot\gamma_p\left(\theta_f-\theta_p\right) \tag{23}$$

$$0=\frac{\partial^2\theta_s}{\partial x^2}+\frac{\partial^2\theta_s}{\partial y^2}+Nhs\cdot\gamma_s\left(\theta_f-\theta_s\right) \tag{24}$$

$$\frac{\partial\psi}{\partial y}\frac{\partial\phi}{\partial x}-\frac{\partial\psi}{\partial x}\frac{\partial\phi}{\partial y}=\frac{1}{Le}\left(\frac{\partial^2\phi}{\partial x^2}+\frac{\partial^2\phi}{\partial y^2}\right)+\frac{Nt}{Le\cdot Nb}\left(\frac{\partial^2\theta_f}{\partial x^2}+\frac{\partial^2\theta_f}{\partial y^2}\right) \tag{25}$$

The corresponding boundary conditions for these equations are given by:

$$\begin{aligned}
&\psi=0,\quad \theta_f=\theta_p=\theta_s=1,\quad Nb\frac{\partial\phi}{\partial x}+Nt\frac{\partial\theta_f}{\partial x}=0\quad \text{on}\quad x=0\\
&\psi=0,\quad \theta_f=\theta_p=\theta_s=0,\quad Nb\frac{\partial\phi}{\partial x}+Nt\frac{\partial\theta_f}{\partial x}=0\quad \text{on}\quad x=1\\
&\psi=0,\quad \frac{\partial\theta_f}{\partial y}=\frac{\partial\theta_p}{\partial y}=\frac{\partial\theta_s}{\partial y}=0,\quad \frac{\partial\phi}{\partial y}=0\quad \text{on}\quad y=0\ \text{and}\ y=1
\end{aligned} \tag{26}$$

here the nine parameters Nr, Nb, Nt, Nhp, Nhs, ε_p, γ_p, γ_s, and Le denote a buoyancy ratio parameter, a Brownian motion parameter, a thermophoresis parameter, the interface heat transfer parameters called as Nield numbers (Vadász, 2008), a modified thermal diffusivity ratio, modified thermal capacity ratios and Lewis number, respectively, which are defined as:

$$\begin{aligned}
&Nr=\frac{(\rho_p-\rho_{f0})C_0}{\rho_{f0}\beta\Delta T(1-C_0)},\quad Nb=\frac{\tau D_B C_0\varepsilon}{\alpha_f},\quad Nt=\frac{\tau D_T\varepsilon\Delta T}{\alpha_f T_c},\quad Nhp=\frac{h_{fp}L^2}{k_f(1-C_0)},\\
&Nhs=\frac{h_{fs}L^2}{k_f(1-C_0)},\quad \varepsilon_p=\frac{\alpha_p\varepsilon}{\alpha_f},\quad \gamma_p=\frac{(1-C_0)(\rho c)_f}{C_0(\rho c)_p},\quad \gamma_s=\frac{k_f(1-C_0)}{k_s(1-\varepsilon)},\quad Le=\frac{\alpha_f}{D_B\varepsilon}
\end{aligned} \tag{27}$$

The physical quantities of interest are the local Nusselt numbers $\underline{Nu_f}$, $\underline{Nu_p}$, $\underline{Nu_s}$, the local Sherwood number Sh and the average Nusselt numbers $\overline{Nu_f}$, $\overline{Nu_p}$, $\overline{Nu_s}$ and Sherwood number $\overline{Sh}$.

The local Nusselt and Sherwood numbers are defined as:

$$Nu_f = -\left(\frac{\partial \theta_f}{\partial x}\right)_{x=0}, \quad Nu_p = -\left(\frac{\partial \theta_p}{\partial x}\right)_{x=0},$$

$$Nu_s = -\left(\frac{\partial \theta_s}{\partial x}\right)_{x=0}, \quad Sh = -\left(\frac{\partial \phi}{\partial x}\right)_{x=0} \tag{28}$$

The average Nusselt and Sherwood numbers are defined as:

$$\overline{Nu_f} = \int_0^1 Nu_f \, dy, \quad \overline{Nu_p} = \int_0^1 Nu_p \, dy,$$

$$\overline{Nu_s} = \int_0^1 Nu_s \, dy, \quad \overline{Sh} = \int_0^1 Sh \, dy \tag{29}$$

It should be noted here that for an analysis of Sherwood numbers it is possible to study only Nusselt numbers because at the left and right vertical walls we have $\partial\phi/\partial x = -(Nt/Nb)(\partial\theta_f/\partial x)$ taking into account boundary conditions for ϕ (Equation (26)). Therefore the further analysis concerning integral parameters will be about only average Nusselt number because $Sh = -(Nt/Nb)Nu_f$ and $\overline{Sh} = -(Nt/Nb)\overline{Nu_f}$.

In the present study the average Nusselt number for the base fluid phase is reported as average $Nu_f = \varepsilon\overline{Nu_f}$ and for the nanoparticles phase as average $Nu_p = \varepsilon_p\overline{Nu_p}$ to explicitly show the non-dimensional heat transfer rare of the corresponding phase.

3. Numerical method and validation

The set of partial differential Equations (21)-(25) subject to the boundary conditions (26) were transformed to weak form and solved using the finite element method (Rao, 2005; Wriggers, 2008). The Lagrange shape function and quadratic elements were utilized in the finite element method (Rao, 2005). The governing equations were fully coupled using damped Newton method (Wriggers, 2008). The solution for the corresponding linear algebraic equations was obtained using a parallel sparse direct solver (Amestoy *et al.*, 2000). The computations are terminated when the residuals for the stream function get bellow 10^{-8}. The present model, in the form of an in-house computational fluid dynamics code, has been validated successfully against the works of Mansour *et al.* (2010), Chamkha and Ismael (2013), Costa (2004), Chamkha *et al.* (2010) and Baytaş and Pop (2002) for steady-state natural convection in an enclosure filled with porous media.

Considering the previous studies, the value of *Nb* and *Nt* are small in the order of 10^{-6}. The Lewis number is large of the order of 10^3 and higher, and *Nr* is higher than unity. The interface heat transfer parameters, Nield numbers (*Nhp* and *Nhs*), are higher than unity (Bhadauria and Agarwal, 2011). The modified thermal diffusivity ratio (ε_p) is about unity and higher, and the modified thermal capacity ratios (γ_p and γ_s,) are order of 10. Here, the results are present for the following typical combination of non-dimensional parameters $Ra = 100$; $Nr = 10.0$; $Nb = 10^{-6}$; $Nt = 10^{-6}$; $Le = 1{,}000$; $\varepsilon = 0.5$; $\varepsilon_p = 1.0$; $Nhp = 10.0$; $Nhs = 10.0$; $\gamma_p = 10.0$ and $\gamma_s = 10.0$.

Table I shows the evaluated Nusselt numbers of various phases for different combinations of the dimensionless interface heat transfer parameters and different grid sizes. Table I shows that the grid size of 150×150 provides accurate results. Hence, all of the calculations were executed using the grid size of 150×150.

Neglecting the effect of nanoparticles ($Nr = Nb = Nt = Nhp = 0$), the present study reduces to the study of LTNE in a porous medium saturated with a pure fluid which was analyzed in the work of Baytaş and Pop (2002). In this case, dividing both sides of Equation (22) by ε, the non-dimensional form of the present study is equivalent with the study of Baytaş and Pop (2002). In this case, a comparison between the computed values of the average Nusselt number and those reported by Baytaş and Pop (2002) is performed in Figure 2. Table II also shows the evaluated values of the average Nusselt

	$Nhp = Nhs = 0$			$Nhp = Nhs = 10$		
Grid size	Nu_f	Nu_s	Nu_p	Nu_f	Nu_s	Nu_p
50×50	2.4733	1.0000	2.7015	2.3083	2.3105	3.3942
100×100	2.4723	1.0000	2.7001	2.3071	2.3120	3.3938
150×150	2.4720	1.00000	2.6998	2.3069	2.3122	3.3937
200×200	2.4719	1.00000	2.6997	2.3068	2.3123	3.3936

Notes: $Ra = 100$; $Nr = 10.0$; $Nb = 10^{-6}$; $Nt = 10^{-6}$; $Le = 1{,}000$; $\varepsilon = 0.5$; $\varepsilon_p = 1.0$; $\gamma_p = 10.0$ and $\gamma_s = 10.0$

Table I. Grid independency test

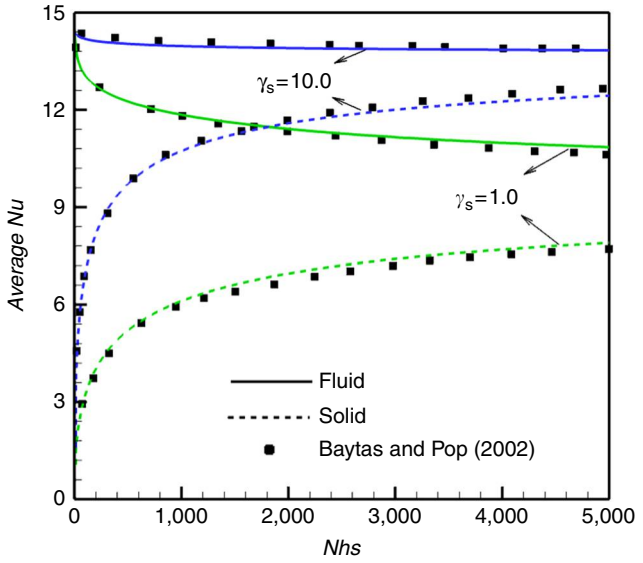

Figure 2. Comparison with the results of Baytaş and Pop (2002) for $\varepsilon = 0.9$ and neglecting nanoparticles

	Baytaş and Pop (2002)						Present study					
	$\gamma_s = 1$		$\gamma_s = 10$		$\gamma_s = 50$		$\gamma_s = 1$		$\gamma_s = 10$		$\gamma_s = 50$	
Nhs	Nu_f	Nu_s	Nu_f	Nu_s	Nu_f	Nu_s	Nu_f	Nu_s	Nu_f	Nu_s	Nu_f	Nu_s
5	14.36	1.26	14.44	2.59	14.64	4.63	14.21	1.26	14.38	2.62	14.46	4.69
10	14.14	1.48	14.51	3.35	14.63	5.76	14.00	1.48	14.34	3.39	14.45	5.83
50	13.43	2.51	14.4	5.70	14.6	8.69	13.36	2.54	14.24	5.77	14.42	8.74
100	13.1	3.18	14.34	6.89	14.58	9.95	13.06	3.23	14.18	6.97	14.41	9.94
500	12.24	5.11	14.16	9.71	14.54	12.42	12.25	5.22	14.03	9.73	14.38	12.20

Notes: $Ra = 1{,}000$; $Nr = Nb = Nt = Nhp = 0$

Table II. Comparison of the average Nusselt number of the hot wall using LTNE model

number of the hot wall for $Ra = 1000$ and compares the results with the data reported by Baytaş and Pop (2002). As seen, there is a good agreement between the results of the present study and the results of Baytaş and Pop (2002).

4. Results and discussion

Figures 3-5 show the contours of the isotherms, concentration of nanoparticles and the nanofluid streamlines for a typical case of LTNE heat natural convection of nanofluids. As seen, there is a significance difference between isotherms of the base fluid, solid matrix and nanoparticles. This difference between the isotherms of three phases is small near isothermal walls where the buoyancy effects and fluid flow are strong. In contrast, the observed difference, between the isotherms of various phases, becomes essential one in the vicinity of the adiabatic horizontal walls where the fluid flow is weak. Figure 4 indicates that the concentration of nanoparticles near the hot vertical wall is low due to the thermophoresis effect. The thermophoresis force acts on the nanoparticles in direction opposite to the temperature gradient, which tends to move nanoparticles from hot to cold. As seen, the concentration of nanoparticles near the cold wall is high. In addition, the weakest concentration of nanoparticles can be seen in the upper left corner of the enclosure (II). Attention to Figure 3 indicates that the temperature gradient near the bottom left corner (I) of the enclosure is higher than that of the corner (II) as the isotherms are denser close to the corner (I). Hence, in the vicinity of the left wall (hot wall), moving from the bottom to top would decrease the strength of the temperature gradients. As the thermophoresis is a direct function of temperature gradient, the intensity of the thermophoresis force would also follow the strength of the temperature gradient. When the nanofluid starts to move upward from the bottom of the hot wall, the thermophoresis tends to push away the nanoparticles in direction away from the hot wall. Hence, the concentration of nanoparticles tends to decrease

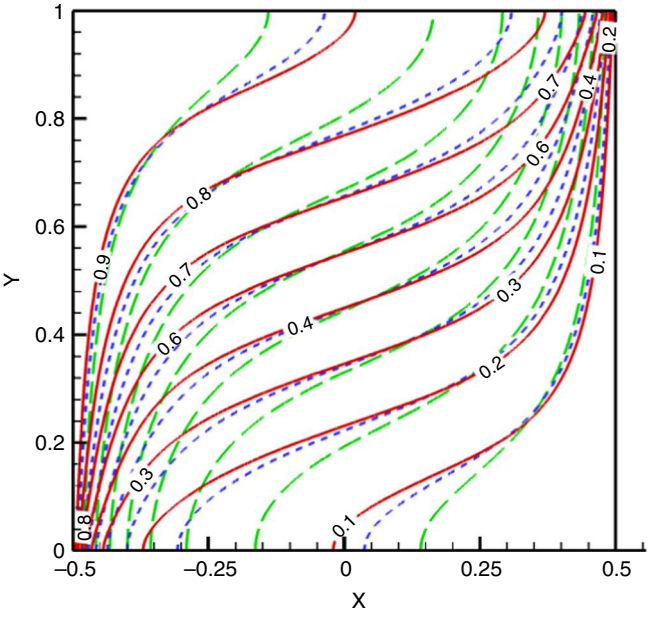

Figure 3.
Isotherms inside the cavity: the solid red lines correspond to the base fluid θ_f; the long dashed green lines correspond to the porous matrix θ_s and the small dashed blue lines correspond to the nanoparticles θ_p

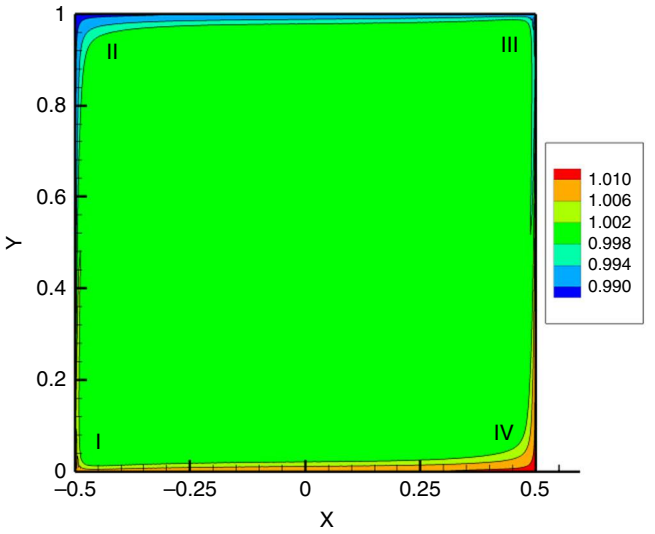

Figure 4.
Contours of the nanoparticles concentrations inside the enclosure

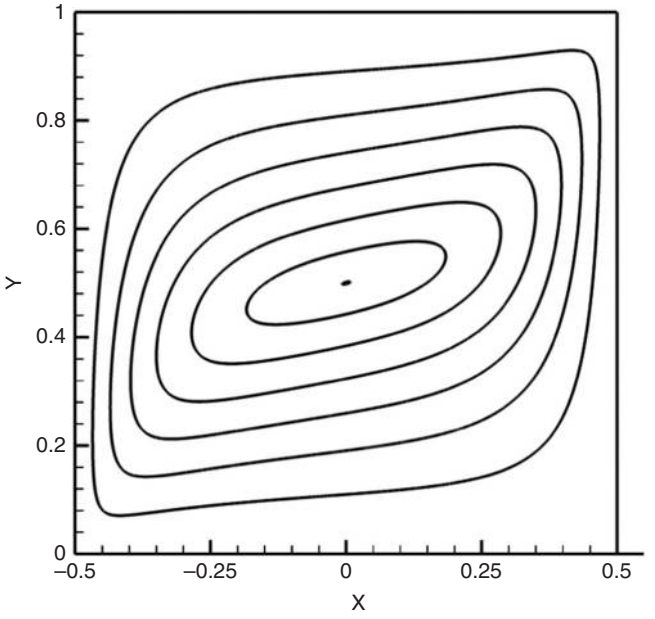

Figure 5.
Streamlines of the nanofluid inside the cavity

towards upward. Then, the flow of nanofluid moves along the horizontal adiabatic top wall until it reaches to the cold wall at right. Thus, the weakest concentration of nanoparticles can be seen in the corner (II) and near the top horizontal adiabatic wall. When the flow of the nanofluid, containing weak concentration of nanoparticles, reaches the cold wall, the temperature gradients get strong again and induce

thermophoresis forces toward the cold wall. Hence, the concentration of nanoparticles increases next to the cold wall, and the strongest concentration of nanoparticles can be seen at the bottom right corner (IV). Figure 4 also shows that the concentration boundary layer of nanoparticles is a thin layer, and the concentration in most parts of the enclosure's core is uniform. The thin concentration boundary layer of nanoparticles is due to the value of Lewis number in nanofluids. The Lewis number shows the ratio of the thermal diffusivity to the nanoparticles diffusion coefficient in nanofluids. For nanofluids, the thermal diffusivity is much higher than the nanoparticles diffusion coefficient, and hence, the Lewis number is a large value. In the theory of the boundary layer, the Lewis number indicates the comparative ratio of the thickness of the thermal boundary layer to the thickness of the concentration boundary layer. The thickness of the thermal boundary layer is mostly affected by the hydrodynamic boundary layer and the buoyancy forces; hence, the thickness of the thermal boundary layer is almost fixed. Therefore, as the consequent of the large values of the Lewis number, the concentration boundary layer is very thin. Figure 5 shows the streamlines of the nanofluid in the enclosure. As seen, the streamlines illustrate the flow circulation of nanofluid inside the cavity. The streamlines are close together near the isothermal walls where the temperature gradients and buoyancy forces are strong. Hence, the velocity near the vertical walls is high and near the core is low.

Figure 6 shows the effect of the buoyancy ratio parameter (Nr) on the isotherms. When nanoparticles migrate from a place into another one, the areas containing high volume fraction of nanoparticles are heavier than that of containing weak concentration of nanoparticles. Hence, the concentration difference would induce the buoyancy force because of the nanoparticles mass transfer. The buoyancy ratio parameter indicates the ratio of buoyancy force due to the mass transfer of nanoparticles to the buoyancy force due to the heat transfer. The increase of Nr

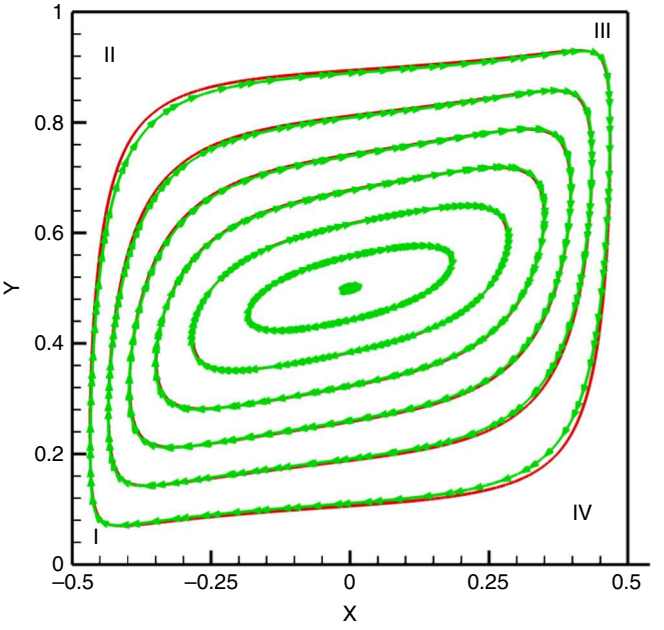

Figure 6.
The streamlines for the nanofluid for $Nr = 0$ (green lines marked with arrows) and $Nr = 30$ (clean red lines)

intensifies the effect of induced buoyancy force due to the mass transfer (migration of nanoparticles). Thus, as seen in Figure 6, the effect of buoyancy ratio parameter (*Nr*) only near the corners of (II) and (IV) is significant. These places correspond to the weakest and strongest concentration of nanoparticle in the enclosure. The difference between the streamlines in the core of the enclosure, where the mass transfer mechanism are negligible, is also negligible.

Figure 7 shows the effect of *Nhs* on the isotherms of the porous matrix. *Nhs* is the interface heat transfer parameter between the fluid phase and the solid phase. Decreasing *Nhs*, the effect of fluid phase on the solid matrix reduces, and hence, for low values of *Nhs* the solid matrix would act as an isolated solid interface in which the temperature would change linearly from hot to cold. Figure 7 also indicates that the isotherms would better follow the non-linear behaviors of the fluid for high values of *Nhs* (dashed green lines). It is also clear that the variation of the interface heat transfer parameter between the fluid phase and the solid phase would significantly affect the isotherms. The effect of *Nhs* on the concentration and fluid phase isotherms was not significant, and hence, they have not been plotted here for the sake of brevity.

Figures 8-10 show the average Nusselt number of the solid, base fluid and nanoparticles phases, respectively. In these figures, the effect of the buoyancy ratio parameter on the average Nusselt numbers for selected values of the solid-fluid interface heat transfer parameter (*Nhs*) is illustrated. As seen, the increase of the buoyancy ratio parameter (*Nr*) leads to the decrease in the magnitude of the average Nusselt number. The observed decrease in the base fluid (Figure 9) and nanoparticles (Figure 10) phases is more significant in comparison with that of the porous solid matrix (Figure 8). The increase of the buoyancy ratio parameter intensifies the induced buoyancy mass transfer effects. As it was seen in Figure 6, these effects are solely important in a small layer close to the vertical isothermal walls. Therefore, the increase

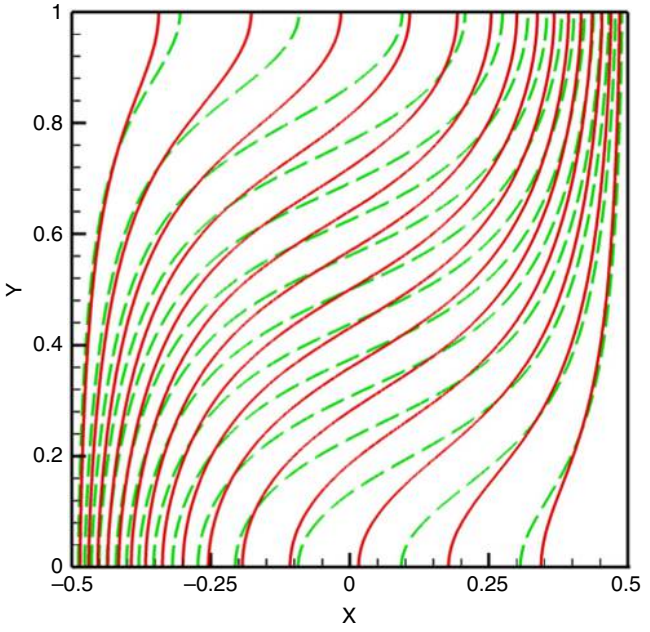

Figure 7.
Isotherms for the porous matrix temperature θ_s for $Nhs = 5$ (solid red lines) and $Nhs = 10$ (the long dashed green lines)

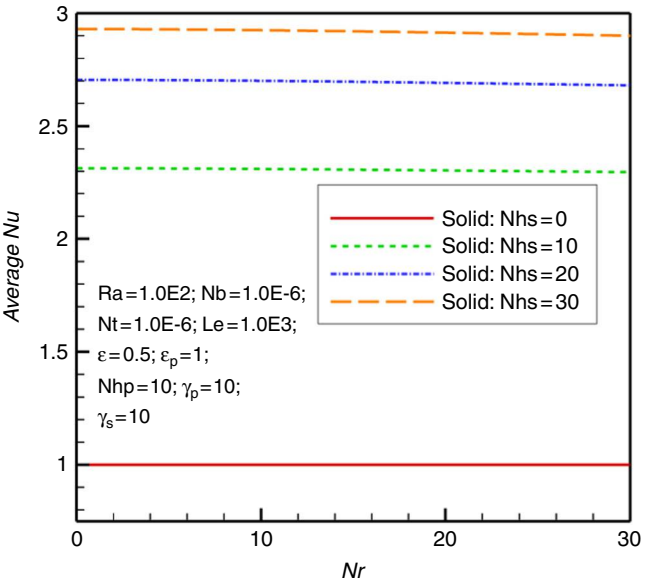

Figure 8.
Average Nusselt number of the porous matrix as a function of the buoyancy ratio parameter (*Nr*) for various values of the solid-fluid interface heat transfer parameter (*Nhs*)

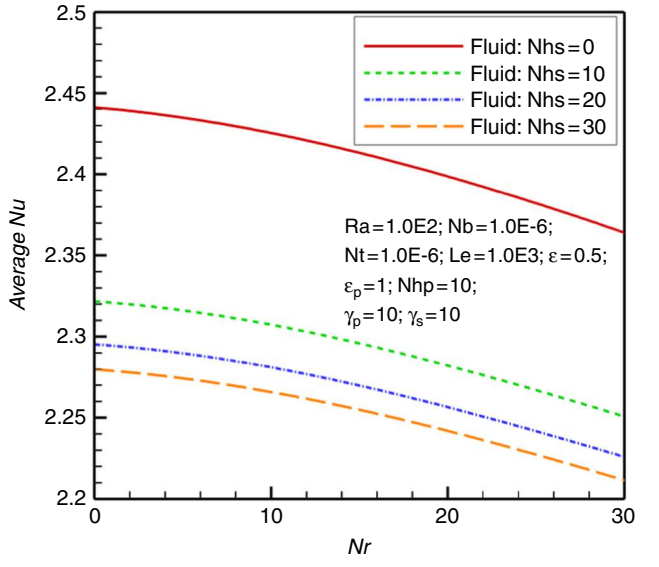

Figure 9.
Average Nusselt number of the fluid as a function of the buoyancy ratio parameter (*Nr*) for different values of the solid-fluid interface heat transfer parameter (*Nhs*)

of the buoyancy ratio parameter boosts the vertical velocity of the fluid in the vicinity of the vertical walls, which results in the decrease of temperature gradient (average Nusselt number). The variation of the buoyancy ratio parameter induces direct significant changes in the buoyancy forces next to the vertical walls which results in

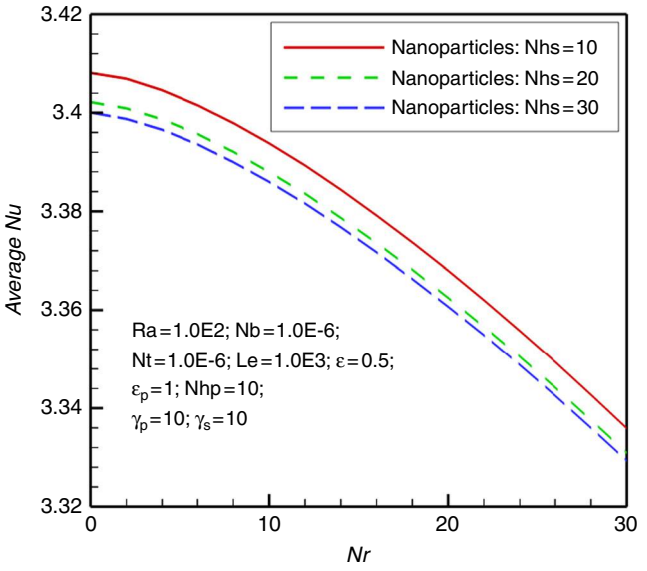

Figure 10. Average Nusselt number of the nanoparticles as a function of the buoyancy ratio parameter (*Nr*) for various values of the solid-fluid interface heat transfer parameter (*Nhs*)

smooth indirect variation of average Nusselt number (temperature gradient) of the base fluid. The variation of the base fluid would consequently affect the temperature gradient of the solid porous medium. However, as seen in Figure 8, this indirect effect is not much significant. Figure 9 indicates that the increase of the solid-fluid interface heat transfer parameter decreases the average Nusselt number for the base fluid phase. In contrast, Figure 8 indicates that the increase of *Nhs* increases the average Nusselt number for the phase of the solid porous matrix. This is because of the fact that the increase of *Nhs* boosts the interaction between the fluid and solid matrix, and consequently tends to reduce the temperature differences between these two phases.

The changes in temperature behavior of nanoparticles are mainly the results of the interaction between nanoparticles and the base fluid. Therefore, the temperature behavior of nanoparticles tends to follow the temperature behavior of the base fluid through interaction with the base fluid. Thus, as seen in Figure 10, the increase of *Nhs* decreases the average Nusselt number for the nanoparticles phase. This is the same trend of behavior as occurred for the base fluid, but the variation of Nusselt number for the nanoparticles phase is smoother than that for the base fluid. This is because of the fact that the variation of *Nhs* directly affects the temperature of the solid porous matrix and the base fluid phases, but the fluctuations of *Nhs* would indirectly change the temperature behavior of the nanoparticles through the variation of base fluid temperature.

Figures 11-13 illustrate the effect of the nanoparticles-fluid interface heat transfer parameter (*Nhp*) on the average Nusselt number of the three phases of the solid porous matrix, base fluid and nanoparticles for various values of the solid-fluid interface heat transfer parameter (*Nhs*). The nanoparticles-fluid interface heat transfer parameter (*Nhp*) indicates the strength of thermal interaction between nanoparticles and the base fluid. As this parameter increases, the interaction between these phases increases.

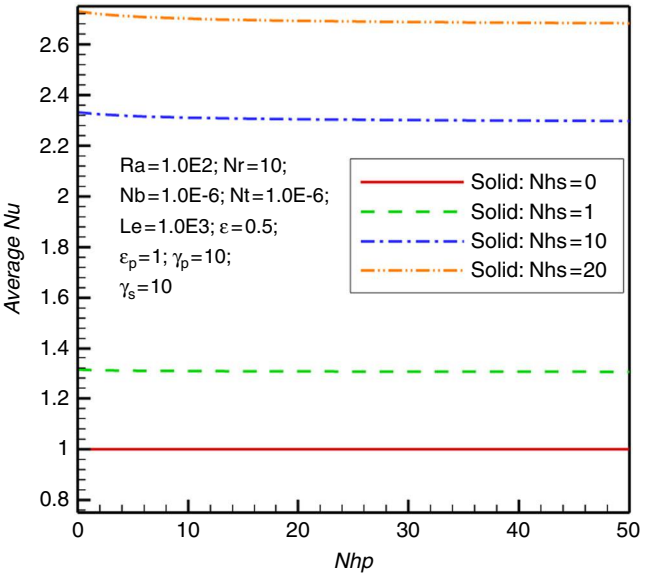

Figure 11.
Average Nusselt number of the porous matrix as a function of the nanoparticles-fluid interface heat transfer parameter (*Nhp*) for various values of solid-fluid interface heat transfer parameter (*Nhs*)

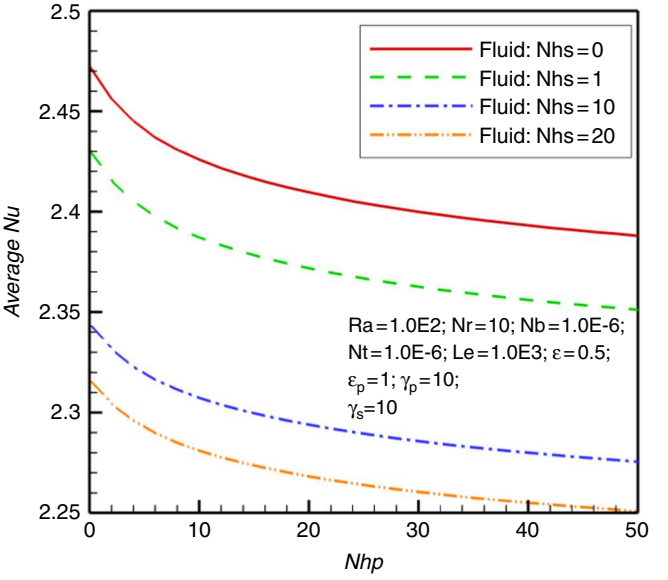

Figure 12.
Average Nusselt number of the fluid phase as a function of the nanoparticles-fluid interface heat transfer parameter (*Nhp*) for various values of solid-fluid interface heat transfer parameter (*Nhs*)

Figure 11 reveals that the effect of variation of *Nhp* on the average Nusselt number is not significant for the solid phase of the porous matrix. This is because the fluctuations of *Nhp* would indirectly affect the temperature behavior of the solid porous phase through the variation of base fluid temperature. This figure in agreement with Figure 8 shows that the increase of *Nhs* increases the average Nusselt number of the solid porous matrix.

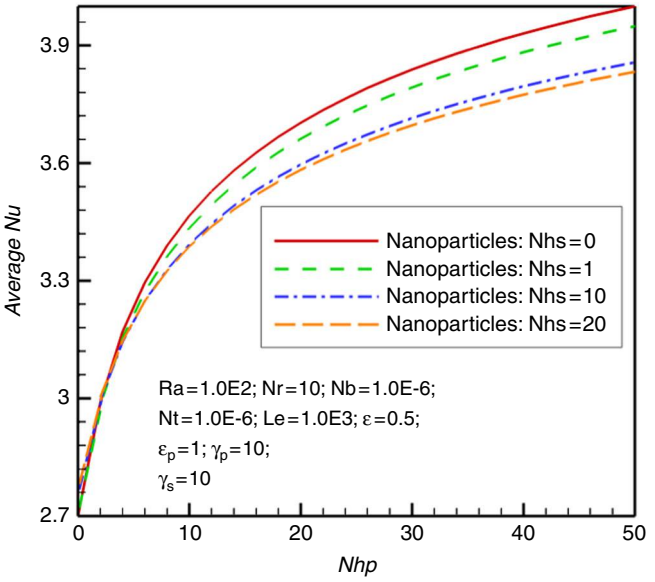

Figure 13.
Average Nusselt number of the nanoparticles phase as a function of the nanoparticles-fluid interface heat transfer parameter (*Nhp*) for various values of solid-fluid interface heat transfer parameter (*Nhs*)

Figures 12 and 13 depict that the increase of *Nhp* tends to reduce the temperature gradient (average Nusselt number) for the base fluid phase and raise the average Nusselt number for the nanoparticles. This is because of the fact that the increase of the interaction between base fluid and nanoparticles tends to reduce the temperature differences between the phases. However, as the heat capacity and volume fraction of nanoparticles are lower than those of the base fluid, the changes in temperature gradient (i.e. reduced Nusselt number) in both sides is not equal. In addition, as it was seen in previous figures, the variation of the solid-fluid interface heat transfer parameter (*Nhs*) also plays an important role in surface temperature gradients of the phases (i.e. Nusselt numbers).

Figures 14-16 illustrate the average Nusselt number of three phases of the solid porous matrix, base fluid and nanoparticles as a function of modified thermal capacity ratio of nanoparticle phase (γ_P) for various values of the modified thermal capacity ratio of the solid matrix of the porous medium phase (γ_s). These figures depict that the increase of the modified thermal capacity ratio of nanoparticle phase (γ_P) increases the average Nusselt number of all phases when the modified thermal capacity ratio of the porous solid matrix (γ_s) is comparatively high. The increase of γ_s would also increase the average Nusselt number for the solid porous matrix and the base fluid, but it induces two different trends of results for the nanoparticle phase. When γ_P is comparatively small ($\gamma_P < 2$), the increase of γ_s decreases the average Nusselt number of nanoparticles, but when γ_P is comparatively large, the increase of γ_s increases the average Nusselt number for the nanoparticles phase. Attention to the governing Equations (21)-(25) indicates that variation of γ_p can reduce or boost the effect of *Nhp* in the heat transfer of nanoparticles phase. Similarly, the variation of γ_s can reduce or intensify the effect of *Nhs* in the phase of the porous solid matrix. Hence, when the magnitude of γ_s is large the temperature of the solid matrix is strongly under influence of the variation of the base fluid phase. In addition, when the magnitude of γ_p is high the

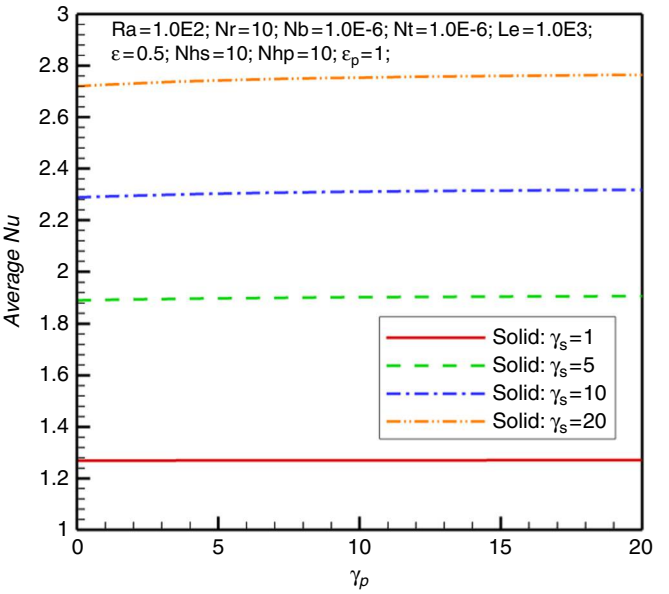

Figure 14.
Average Nusselt number of the porous matrix as a function of γ_p for various values of γ_s

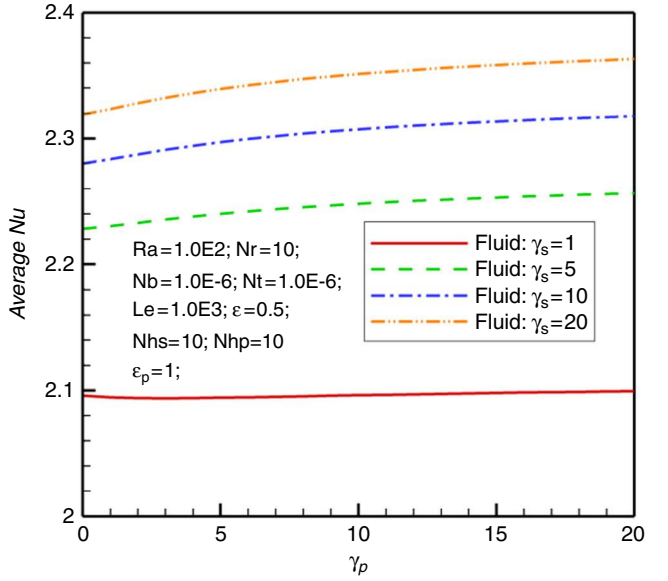

Figure 15.
Average Nusselt number of the fluid phase as a function of γ_p for various values of γ_s

temperature of nanoparticles is under the strong influence of the base fluid phase. Therefore, in the case of the large values of γ_p and γ_s, the temperatures (as well as the Nusselt numbers) should follow the behavior of the base fluid. Figure 15 reveals that the variation of γ_p can smoothly change the magnitude of the average Nusselt number of the base fluid. However, it induces strong effects on the magnitude of the Nusselt

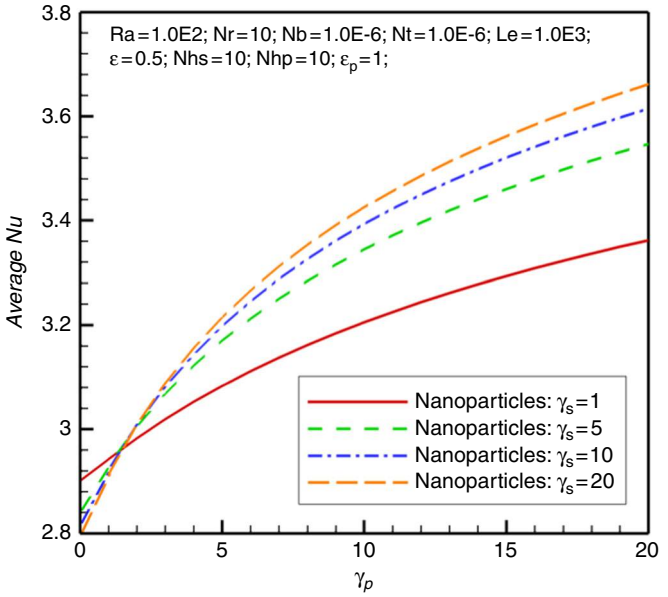

Figure 16. Average Nusselt number of the fluid phase as a function of γ_p for various values of γ_s

number of the nanoparticles phase. Figure 14 indicates that the variation of γ_p does not show significant effects on the variation of the Nusselt number of the solid porous matrix. This is because of the fact that the variation of γ_p would indirectly change the temperature gradients of the base fluid through the variation of nanoparticles temperatures. Then, the smooth variation of the base fluid temperature would change the temperatures of the solid matrix of the porous medium. Figure 14 shows that the variation of γ_s induces significant changes in the magnitude of the average Nusselt number of the solid-matrix phase. As the magnitude of γ_s increases, the effect of interaction between solid-base fluid phases (i.e. *Nhs*) intensifies in the solid porous matrix side. In Figure 8, it was observed that the increase of *Nhs* tends to increase the average Nusselt number of the solid matrix of porous medium. Here, the increase of γ_s ($\gamma_s = 10$) has intensified this effect and increased the reduced Nusselt number.

As mentioned, Figure 15 shows that the increase of γ_s increases the reduced Nusselt number for the base fluid. Indeed, the increase of γ_s indirectly affects the Nusselt number of the base fluid through the variation of the temperature of the solid porous matrix. When γ_p is large any changes in temperature of the fluid would be boosted for nanoparticles, and the temperature of the base fluid dominantly changes the temperature of nanoparticles. Hence, as seen in Figure 16, the increase of γ_s raises the magnitude of the average Nusselt number for large values of γ_p. Indeed, this trend of results follows the trend of results of Figure 15. In contrast, when γ_p is small, the variation of the temperature of the base fluid could be neglected, and the changes in temperature of nanoparticles would be the results of the diffusive term as well as the velocity of the base fluid. It is clear that the diffusive term is not under influence of γ_s. Therefore, the changes in the average Nusselt number of nanoparticles correspond to velocity (advection) terms for the case of small values of γ_p. Figure 15 indicates as γ_s

increases the average Nusselt number for the base fluid (Figure 15), and consequently, the velocity increases. The increment of the velocity reduces the temperature gradient of nanoparticles. Hence, as seen in Figure 16, the increase of γ_s reduces the magnitude of the average Nusselt number for small values of γ_p.

5. Conclusion

The natural convective flow and heat transfer of nanofluids in a square enclosure filled with a homogenous porous medium saturated with a nanofluid is theoretically analyzed. The nanofluid and porous medium are considered in LTNE. The nanoparticles in the nanofluid are also subject to drift flux due to the Brownian motion and thermophoresis forces. The governing equations in non-dimensional form were solved using a finite element code. The results for the heat transfer of nanofluids were reported in the form of the Nusselt number graphs for three phases of solid porous matrix, base fluid and nanoparticles. The main outcomes of the results of the present study can be summarized as follows:

(1) The increase of buoyancy ratio parameter (*Nr*) decreases the magnitude of average Nusselt number.

(2) The increase of the nanoparticles-fluid interface heat transfer parameter (*Nhp*) increases the average Nusselt number for nanoparticles and decreases the average Nusselt number for the base fluid. Similarly, the increase of the solid-fluid interface heat transfer parameter (*Nhs*) increases the average Nusselt number for the porous matrix and the nanoparticles and decreases the average Nusselt number for the base fluid. The effect of variation of *Nhp* on the average Nusselt number of the porous matrix is not significant.

(3) The increase of the modified thermal capacity ratio of nanoparticle phase (γ_P) increases the average Nusselt number of all phases when the modified thermal capacity ratio of the porous solid matrix (γ_s) is comparatively high. Therefore, nanofluids with large values of modified thermal capacity ratio are of interest for heat transfer applications.

(4) The increase of the modified thermal capacity ratio of the porous solid matrix (γ_s) raises the average Nusselt number for all phases when the modified thermal capacity ratio nanoparticle phase (γ_P) is comparatively high. In practical cases, the values of γ_P are large, and hence, in heat transfer applications, the mixtures of nanofluids and porous matrix with high values of γ_s are of interest.

References

Abu-Nada, E. and Chamkha, A.J. (2010), "Effect of nanofluid variable pzroperties on natural convection in enclosures filled with an CuO-EG-water nanofluid", *International Journal of Thermal Sciences*, Vol. 49 No. 12, pp. 2339-2352.

Amestoy, P.R., Duff, I.S. and L'Excellent, J.Y. (2000), "Multifrontal parallel distributed symmetric and unsymmetric solvers", *Computer Methods in Applied Mechanics and Engineering*, Vol. 184 No. 2, pp. 501-520.

Basak, T. and Chamkha, A.J. (2012), "Heatline analysis on natural convection for nanofluids confined within square cavities with various thermal boundary conditions", *International Journal of Heat and Mass Transfer*, Vol. 55 Nos 21-22, pp. 5526-5543.

Baytaş, A.C. and Pop, I. (1999), "Free convection in oblique enclosures filled with a porous medium", *International Journal of Heat Mass Transfer*, Vol. 42 No. 6, pp. 1047-1057.

Baytaş, A.C. and Pop, I. (2001), "Natural convection in a trapezoidal enclosure filled with a porous medium", *International Journal of Engineering Science*, Vol. 39 No. 2, pp. 125-134.

Baytaş, A.C. and Pop, I. (2002), "Free convection in a square porous cavity using a thermal nonequilibrium model", *International Journal of Thermal Sciences*, Vol. 41 No. 9, pp. 861-870.

Bhadauria, B.S. and Agarwal, S. (2011), "Convective transport in a nanofluid saturated porous layer with thermal non equilibrium model", *Transport in Porous Media*, Vol. 88 No. 1, pp. 107-131.

Buongiorno, J. (2006), "Convective transport in nanofluids", *Journal of Heat Transfer*, Vol. 128 No. 3, p. 240.

Chamkha, A.J. and Abu-Nada, E. (2012), "Mixed convection flow in single- and double-lid driven square cavities filled with water-Al_2O_3 nanofluid: effect of viscosity models", *European Journal of Mechanics – B/Fluids*, Vol. 36, pp. 82-96.

Chamkha, A.J. and Ismael, M.A. (2013), "Conjugate heat transfer in a porous cavity heated by a triangular thick wall", *Numerical Heat Transfer, Part A: Applications*, Vol. 63 No. 2, pp. 144-158.

Chamkha, A.J., Mansour, M.A. and Ahmed, S.E. (2010), "Double-diffusive natural convection in inclined finned triangular porous enclosures in the presence of heat generation/absorption effects", *Heat Mass Transfer*, Vol. 46 No. 7, pp. 757-768.

Choi, C., Yoo, H.S. and Oh, J.M. (2008), "Preparation and heat transfer properties of nanoparticle-in-transformer oil dispersions as advanced energy-efficient coolants", *Current Applied Physics*, Vol. 8 No. 6, pp. 710-712.

Choi, E., Chakma, A. and Nandakumar, K. (1998), "A bifurcation study of natural convection in porous media with internal heat sources: the non-Darcy effects", *International Journal of Heat and Mass Transfer*, Vol. 41 No. 2, pp. 383-392.

Costa, V.A.F. (2004), "Double-diffusive natural convection in parallelogrammic enclosures filled with fluid-saturated porous media", *International Journal of Heat and Mass Transfer*, Vol. 47 No. 12, pp. 2699-2714.

Hirota, K., Sugimoto, M., Kato, M., Tsukagoshi, K., Tanigawa, T. and Sugimoto, H. (2010), "Preparation of zinc oxide ceramics with a sustainable antibacterial activity under dark conditions", *Ceramics International*, Vol. 36 No. 2, pp. 497-506.

Ingham, D.B. and Pop, I. (Eds) (2005), *Transport Phenomena in Porous Media III*, Elsevier, Oxford.

Keblinski, P. and Cahill, D.G. (2005), "Comment on model for heat conduction in nanofluids", *Physical Review Letters*, Vol. 95 No. 20, pp. 209-401.

Khanafer, K. and Vafai, K. (2011), "A critical synthesis of thermophysical characteristics of nanofluids", *International Journal of Heat and Mass Transfer*, Vol. 54 No. 19, pp. 4410-4428.

Kuznetsov, A.V. and Nield, D.A. (2010), "Effect of local thermal non-equilibrium on the onset of convection in a porous medium layer saturated by a nanofluid", *Transport in Porous Media*, Vol. 83 No. 2, pp. 425-436.

Kuznetsov, A.V. and Nield, D.A. (2013), "The Cheng-Minkowycz problem for natural convective boundary layer flow in a porous medium saturated by a nanofluid: a revised model", *International Journal of Heat and Mass Transfer*, Vol. 65, pp. 682-685.

Mansour, M.A., Chamkha, A.J., Mohamed, R.A., El-Aziz, M.A. and Ahmed, S.E. (2010), "MHD natural convection in an inclined cavity filled with a fluid saturated porous medium with heat source in the solid phase", *Nonlinear Analysis: Modelling and Control*, Vol. 15 No. 1, pp. 55-70.

Nasrin, R., Alim, M.A. and Chamkha, A.J. (2012), "Buoyancy-driven heat transfer of water-Al_2O_3 nanofluid in a closed chamber: effects of solid volume fraction, Prandtl number and aspect ratio", *International Journal of Heat and Mass Transfer*, Vol. 55 Nos 25-26, pp. 7355-7565.

Nasrin, R., Chamkha, A.J. and Alim, M.A. (2014), "Modeling of mixed convective heat transfer utilizing nanofluid in a double lid-driven chamber with internal heat generation", *International Journal for Numerical Methods in Heat and Fluid Flow*, Vol. 24 No. 1, pp. 36-57.

Nield, D.A. and Kuznetsov, A.V. (2009a), "The Cheng–Minkowycz problem for natural convective boundary-layer flow in a porous medium saturated by a nanofluid", *International Journal of Heat Mass Transfer*, Vol. 52 No. 25, pp. 5792-5795.

Nield, D.A. and Kuznetsov, A.V. (2009b), "Thermal instability in a porous medium layer saturated by a nanofluid", *International Journal of Heat and Mass Transfer*, Vol. 52 No. 25, pp. 5796-5801.

Nield, D.A. and Kuznetsov, A.V. (2014), "Thermal instability in a porous medium layer saturated by a nanofluid: a revised model", *International Journal of Heat and Mass Transfer*, Vol. 68, pp. 211-214.

Rao, S.S. (2005), *The Finite Element Method in Engineering*, Butterworth-Heinemann, Oxford.

Saidur, R., Leong, K.Y. and Mohammad, H.A. (2011), "A review on applications and challenges of nanofluids", *Renewable and Sustainable Energy Reviews*, Vol. 15 No. 3, pp. 1646-1668.

Sheremet, M.A. and Pop, I. (2014), "Conjugate natural convection in a square porous cavity filled by a nanofluid using Buongiorno's mathematical model", *International Journal of Heat and Mass Transfer*, Vol. 79, pp. 137-145.

Sheremet, M.A. and Pop, I. (2015), "Natural convection in a wavy porous cavity with sinusoidal temperature distributions on both side walls filled with a nanofluid: Buongiorno's mathematical model", *Journal of Heat Transfer*, Vol. 137 No. 7, p. 072601.

Tzou, D.Y. (2008a), "Instability of nanofluids in natural convection", *Journal of Heat Transfer*, Vol. 130 No. 7, p. 072401.

Tzou, D.Y. (2008b), "Thermal instability of nanofluids in natural convection", *International Journal of Heat and Mass Transfer*, Vol. 51 No. 11, pp. 2967-2979.

Vadász, P. (Ed.) (2008), *Emerging Topics in Heat and Mass Transfer in Porous Media: From Bioengineering and Microelectronics to Nanotechnology*, Vol. 22, Springer Science & Business Media, Berlin.

Varol, Y., Oztop, H.F. and Pop, I. (2008), "Numerical analysis of natural convection in an inclined trapezoidal enclosure filled with a porous medium", *International Journal Thermal Sciences*, Vol. 47 No. 10, pp. 1316-1331.

Wriggers, P. (2008), *Nonlinear Finite Element Methods*, Springer Science & Business Media, Berlin.

Zhang, L., Ding, Y., Povey, M. and York, D. (2008), "ZnO nanofluids–a potential antibacterial agent", *Progress in Natural Science*, Vol. 18 No. 8, pp. 939-944.

Corresponding author
Ioan Pop can be contacted at: popm.ioan@yahoo.co.uk